

Creating and detecting poor man's Majorana bound states in interacting quantum dots

Athanasios Tsintzis,¹ Rubén Seoane Souto,^{1,2} and Martin Leijnse^{1,2}

¹*Division of Solid State Physics and NanoLund, Lund University, S-221 00 Lund, Sweden*

²*Center for Quantum Devices, Niels Bohr Institute,
University of Copenhagen, DK-2100 Copenhagen, Denmark*

(Dated: November 29, 2022)

We propose and theoretically investigate an alternative way to create the poor man's Majorana bound states (MBSs) introduced in Phys. Rev. B **86**, 134528 (2012). Our proposal is based on two quantum dots (QDs) with strong electron-electron interactions that couple via a central QD with proximity-induced superconductivity. In the presence of spin-orbit coupling and a magnetic field, gate control of all three QDs allows tuning the system into sweet spots with one MBS localized on each outer dot. We quantify the quality of these MBSs and show how it depends on the Zeeman energy and interaction strength. We also show how nonlocal transport spectroscopy can be used to identify sweet spots with high MBS quality. Our results provide a path for investigating MBS physics in a setting that is free of many of the doubts and uncertainties that plague other platforms.

Introduction. The realization of Majorana bound states (MBSs) [1–4] is one of the most heavily pursued goals in condensed matter physics. The motivation is their theoretically predicted nonabelian and nonlocal properties. In addition to being of fundamental interest as a new physics phenomenon, these properties allow for protected ways to store and manipulate quantum information [5]. The simplest toy model where MBSs arise is the Kitaev model [6], a tight-binding chain with spinless electrons and p -wave superconducting pairing. An explosion in experimental activities was motivated by various theoretical proposals showing that different quantum systems can be engineered such that the Kitaev model arises as an effective description of the low-energy degrees of freedom [7–13].

By now, experiments have revealed signatures consistent with MBSs in several of the proposed platforms, see Refs. [12, 14–22] for a few examples. However, it has also become increasingly clear that the disorder that plagues all real materials can give rise to other, nontopological, states that can provide an alternative explanation for most experimental observations [23–33]. So far, the nonabelian and nonlocal properties of MBSs have not been experimentally demonstrated.

One way to avoid the problem of imperfect materials is to engineer an artificial Kitaev chain in quantum dots (QDs) coupled via narrow superconducting regions [34]. In fact, it was shown in Ref. [35] that two QDs are enough to obtain MBSs, named poor man's MBSs because they possess all the properties of MBSs but only exist at fine-tuned sweet spots in parameter space. The poor man's MBSs system closely resembles Cooper pair splitter devices [36–39], but requires both strong crossed Andreev reflection (CAR) and the ability to fine-tune either the spin-orbit coupling strength or the angle between non-collinearly polarized QD spins. In addition, given the lack of topological protection, it is unclear how close one can come to ideal MBSs in a realistic system with finite Zeeman energy and electron-electron interactions on the

QDs.

In this work, we show a way to overcome the difficulties and uncertainties associated with the original proposal for poor man's MBSs. A key ingredient is to couple the QDs via a central QD which is, in turn, strongly proximitized by a superconductor. The advantage is that gating the center QD provides control of the relative amplitudes of CAR and elastic cotunneling (ECT), which allows realizing poor man's MBSs with a constant spin-orbit coupling (or a constant finite angle between the effective magnetic fields on the two QDs). The underlying physics is the same as a recent proposal for coupling the QDs via an Andreev bound state [40]. We analyze the role of finite Zeeman splitting (including both spin states on all three QDs) as well as strong Coulomb interactions. We show that sweet spots in parameter space exist where the system exhibits three characteristics that are prerequisites for MBSs with nonabelian properties: (*i*) degenerate even and odd (electron number) parity ground states; (*ii*) a substantial gap to the excited states; (*iii*) localized MBSs of high quality, which we quantify with the Majorana polarization (MP) [41–43]. Our results also show how the MP depends on the interaction strength and Zeeman energy. This is important because there are regions in parameter space associated with apparent sweet spots that fulfill (*i*) and (*ii*), but have poor MP. Finally, we calculate the nonlocal transport signatures of the interacting system, and show that they can be used to identify sweet spots and distinguish between true sweet spots and apparent sweet spots with low MP.

While finalizing the present manuscript, a report of experimental signatures consistent with poor man's MBSs appeared [44] based on the Andreev bound state coupling proposed in Ref. [40]. The experiments were compared with a non-interacting model with infinite Zeeman energy, similar to Ref. [35]. The ground-state properties of interacting double QDs harbouring poor man's MBSs have also been investigated in Refs. [45–47].

Proposed device and model. To create and detect poor

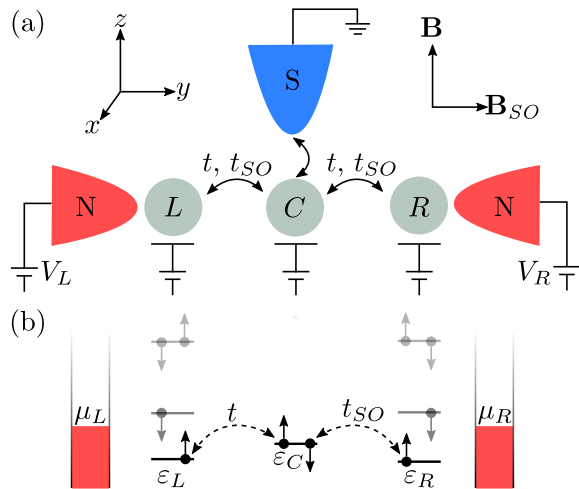


FIG. 1. (a) Setup with three QDs (L, C, R) coupled via spin-conserving tunneling t and (spin-orbit induced) spin-flip tunneling t_{SO} . QD C is strongly coupled to a grounded superconductor. \mathbf{B} is an external Zeeman field and \mathbf{B}_{SO} is a spin-orbit field. (b) QD orbitals ϵ_j and examples of tunnel processes. Electron-electron interactions increase the energy cost of occupying a QD with two electrons. Two normal leads with chemical potentials $\mu_{L,R}$ (controlled by voltages $V_{L,R}$) couple to QDs L and R and can be used for tunnel spectroscopy.

man's MBSs, we propose a device with three coupled QDs. The setup is shown in Fig. 1(a), while Fig. 1(b) shows a sketch of the involved energies and tunnel processes. The system is described by the Hamiltonian [excluding for now the normal (N) leads]:

$$\begin{aligned}
 H_{QDs} = & \sum_{\sigma,j} \epsilon_j n_{j\sigma} + \sum_j U_j n_{j\uparrow} n_{j\downarrow} + \sum_j E_{Zj} n_{j\downarrow} \\
 & + \sum_{\sigma,j \neq C} [t_j d_{j\sigma}^\dagger d_{C\sigma} + h.c.] \\
 & + \sum_{j \neq C} [t_j^{SO} d_{j\uparrow}^\dagger d_{C\downarrow} - t_j^{SO} d_{j\downarrow}^\dagger d_{C\uparrow} + h.c.] \\
 & + \Delta [d_{C\uparrow}^\dagger d_{C\downarrow}^\dagger + h.c.]. \quad (1)
 \end{aligned}$$

Here, $d_{j\sigma}^\dagger$ creates an electron with spin $\sigma = \uparrow, \downarrow$ in QD $j = L, C, R$ with occupation $n_{j\sigma} = d_{j\sigma}^\dagger d_{j\sigma}$, single particle orbital energy ϵ_j , charging energy U_j and Zeeman energy E_{Zj} . t_j is the amplitude for spin-conserving tunneling between QDs $j = L, R$ and QD C , while t_j^{SO} is the amplitude for spin-flip tunneling which results from a spin-orbit interaction with spin-orbit field \mathbf{B}_{SO} along the y -axis, perpendicular to the external Zeeman field \mathbf{B} chosen here to be along the z -axis [48]. We include the proximity-induced superconductivity on QD C through a pairing term of amplitude Δ , which is a reasonable approximation for energies below the superconducting gap [49–52].

Relation to the original poor man's MBS model. In the original model for poor man's MBSs [35], a superconductor mediates two different types of couplings between two

fully spin-polarized QDs: CAR and ECT – corresponding respectively to the pairing and hopping terms in the Kitaev model [6]. The CAR and ECT amplitudes scale in the same way with the QD-superconductor coupling strength, but their ratio can be controlled via the angle between the QD spins. The MBS sweet spot occurs when the CAR and ECT amplitudes are equal and both QD levels are at zero energy (i.e., aligned with the chemical potential of the superconductor). At this point, the Kitaev chain hosts one MBS fully localized on each end site; then two sites – or two QDs – suffice to have spatially separated MBSs.

The relation between H_{QDs} in Eq. (1) and the simple poor man's MBS model is most easily understood in the regime where $|\epsilon_j|, |t_j|, |t_j^{SO}|, |E_{ZC}| \ll |\Delta|, |E_{ZL,R}|$ (although our future analyses will not be limited to this regime). Then, in the ground state, QDs L and R are occupied by zero or one electron each, while QD C is in a superposition of empty and doubly occupied (single occupation being suppressed by the large superconducting pairing). Second order perturbation theory in t_j and t_j^{SO} gives a coupling between QDs L and R , both through ECT ($\propto t_L t_R$) and CAR ($\propto t_L t_R^{SO} + t_R t_L^{SO}$, as the singlet nature of the Cooper pairs means that a spin flip is needed to populate the lowest spin state of each QD). H_{QDs} conserves the parity (even or odd) of the total electron number. Couplings within the even (odd) parity sector are mediated by CAR (ECT) which therefore lowers the energy of the even (odd) parity ground state. However, because of interference between different tunnel processes, the amplitudes of CAR and ECT depend differently on ϵ_C , such that ECT is suppressed around $\epsilon_C = 0$. A similar control of the CAR and ECT relative amplitudes can be achieved using a closely related model with an Andreev bound state mediating the coupling between two QDs, as proposed in Ref. [40] and exploited in the experiments presented in Refs [44, 53].

Based on the original poor man's MBS model, a sweet spot is expected when the ECT and CAR amplitudes are equal and $\epsilon_L = \epsilon_R = 0$. To some degree this still holds in our model for finite E_{Zj} and U_j , but we need to compensate for renormalizations of $\epsilon_{L,R}$ due to the coupling to QD C . Away from the perturbative regime (in t_j, t_j^{SO}), the concepts of CAR and ECT are no longer well-defined, but the processes coupling states within the even parity sector and within the odd parity sector still depend differently on ϵ_C .

Sweet spots and MBS quality. Throughout the rest of the paper we, for simplicity, consider a symmetric system, $t_L = t_R = t$, $t_L^{SO} = t_R^{SO} = t_{SO}$, $U_L = U_R = U$, $E_{ZL} = E_{ZR} = E_Z$. We assume that the strong coupling of QD C to the grounded superconductor has quenched its charging energy by a combination of capacitive effects and tunnel-induced renormalization, and reduced its Zeeman splitting (because of the small g-factor of the superconductor). We therefore take $U_C = E_C = 0$ but have verified that relaxing these assumptions does not qualitatively change the results, see SI [54]. Unless otherwise

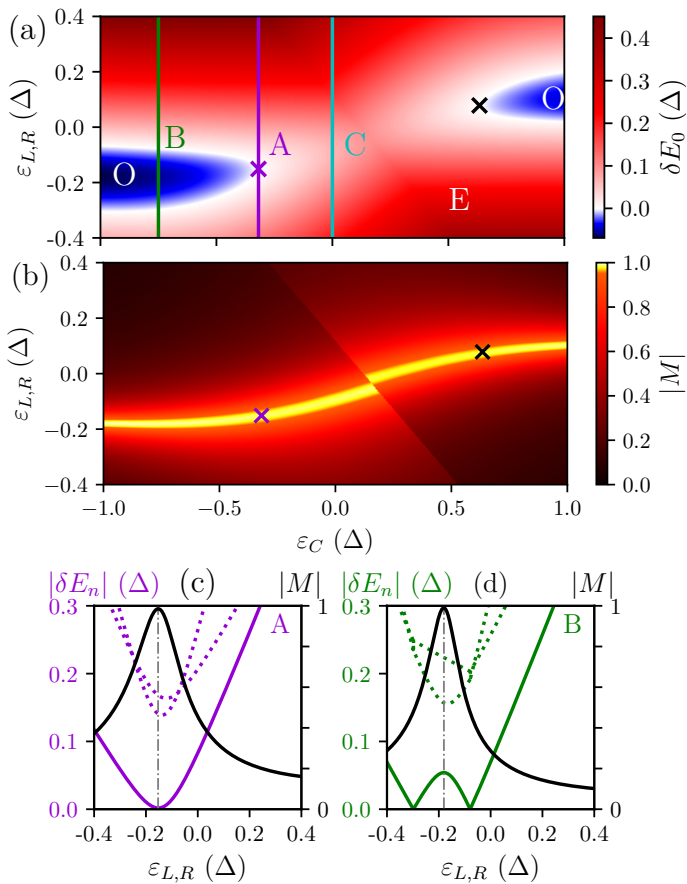


FIG. 2. (a) δE_0 as a function of $\epsilon_L = \epsilon_R$ and ϵ_C . Cuts marked A, B and C are explored in (c, d) and in Fig. 3, while O and E mark regions where the global ground state has odd and even parity, respectively. The purple cross marks the $\epsilon_C < 0$ sweet spot at $\epsilon_C \approx -0.319\Delta$, $\epsilon_L = \epsilon_R \approx -0.151\Delta$, while the $\epsilon_C > 0$ sweet spot is marked by the black cross at $\epsilon_C \approx 0.634\Delta$, $\epsilon_L = \epsilon_R \approx 0.0785\Delta$. (b) $|M|$ as a function of $\epsilon_L = \epsilon_R$ and ϵ_C . The crosses mark the same points as in (a). (c) $|\delta E_n|$ (left axis, purple lines) as a function of $\epsilon_L = \epsilon_R$ along cut A (purple line) in (a). The lowest excited state (full line) has different parity (odd in this case) than the ground state (even in this case); one of the two higher excited states shown (dotted lines) has even parity and the other odd. The black line shows $|M|$ (right axis) as a function of $\epsilon_L = \epsilon_R$ along cut A in (a). (d) Same as (c) but along cut B (green line) in (a). The vertical dash-dotted lines in (c) and (d) indicate the maximum of $|M|$.

stated, we choose the following values for the remaining parameters ($e = \hbar = k_B = 1$): $U = 5\Delta$, $t = 0.5\Delta$, $t_{SO} = 0.2t$, $E_Z = 1.5\Delta$.

We first focus on $\delta E_0 = E^O - E^E$, the energy difference between the odd and even parity ground states of H_{QDs} in Eq. (1). As explained above, ϵ_C affects the even and odd ground state energies by changing the relative strengths of couplings within the even and odd parity sectors. For $|\epsilon_C| < |\Delta|$ and $\epsilon_L = \epsilon_R$, the ground state is dominated by an even electron number on QD C . For large positive $\epsilon_{L,R}$, QDs L and R are both mainly empty,

and the global ground state of all three QDs thus has even parity. For negative $\epsilon_{L,R}$ with $|\epsilon_{L,R}| < U$, the global ground state is also even, because it is dominated by single occupations of both QDs L and R .

The above behavior is seen in Fig. 2(a) which shows δE_0 as a function of ϵ_C and $\epsilon_L = \epsilon_R$. When changing $\epsilon_{L,R}$ along a vertical cut we start and end with an even parity ground state, but if $|\epsilon_C|$ is large enough there is a region in between with an odd parity ground state [blue color in Fig. 2(a)]. This happens for values of ϵ_C such that couplings within the odd parity sector are stronger than those within the even parity sector. There are two values of ϵ_C where this region reduces to a point as a function of $\epsilon_{L,R}$ [marked with purple and black crosses in Fig. 2(a)] and we will see that these points are the closest we come to sweet spots with MBSs.

From Fig. 2(a) we see that we have lines in parameter space with degenerate even and odd parity ground states (white color). To determine whether these degeneracies are associated with MBSs, we quantify the MBS quality using the MP [41]. In our case, it corresponds to the degree that a Hermitian operator localized on one of the outer QDs $j \neq C$ can switch between the lowest energy even and odd states:

$$M_j = \frac{\sum_{\sigma} (w_{\sigma}^2 - z_{\sigma}^2)}{\sum_{\sigma} (w_{\sigma}^2 + z_{\sigma}^2)}, \quad (2)$$

$$w_{\sigma} = \langle O | (d_{j\sigma} + d_{j\sigma}^{\dagger}) | E \rangle, \quad (3)$$

$$z_{\sigma} = \langle O | (d_{j\sigma} - d_{j\sigma}^{\dagger}) | E \rangle, \quad (4)$$

where $|E\rangle$ ($|O\rangle$) is the lowest energy even (odd) parity state. This definition guarantees that $0 \leq |M_j| \leq 1$, where $|M_j| = 1$ would indicate a single MBS perfectly localized on QD j , with no other MBS operator having any weight there. For the presented results, $M_L = -M_R$ and in the following we drop the index j and focus on $|M_L| = |M_R| = |M|$

Figure 2(b) shows $|M|$ plotted over the same range in ϵ_C and $\epsilon_L = \epsilon_R$ used in Fig. 2(a). There is a line where $|M|$ comes very close to 1, but this line only coincides with an even-odd degeneracy at two isolated points (marked with purple and black crosses). The discontinuity in $|M|$ arises because the two lowest energy odd-parity states undergo a crossing. This turns into an avoided crossing for $\epsilon_L \neq \epsilon_R$ and occurs in a regime far from even/odd ground state degeneracy where the MP has little meaning.

Figures 2(c) and (d) show $|M|$ together with $|\delta E_n|$ and the excitation energies above the global ground state ($|\delta E_n|$, $n \geq 1$) as a function of $\epsilon_L = \epsilon_R$ for two different values of ϵ_C [purple and green cuts in Fig. 2(a)]. Along both cuts, we find even/odd degeneracies with a substantial separation to excited states. However, it is only in Fig. 2(c) that this degeneracy coincides with a large $|M|$ (≈ 0.986), while in Fig. 2(d) the peak in $|M|$ lies in between the two degeneracy points. Similar results are found for the region where $\epsilon_C > 0$.

We also investigate another important property of the

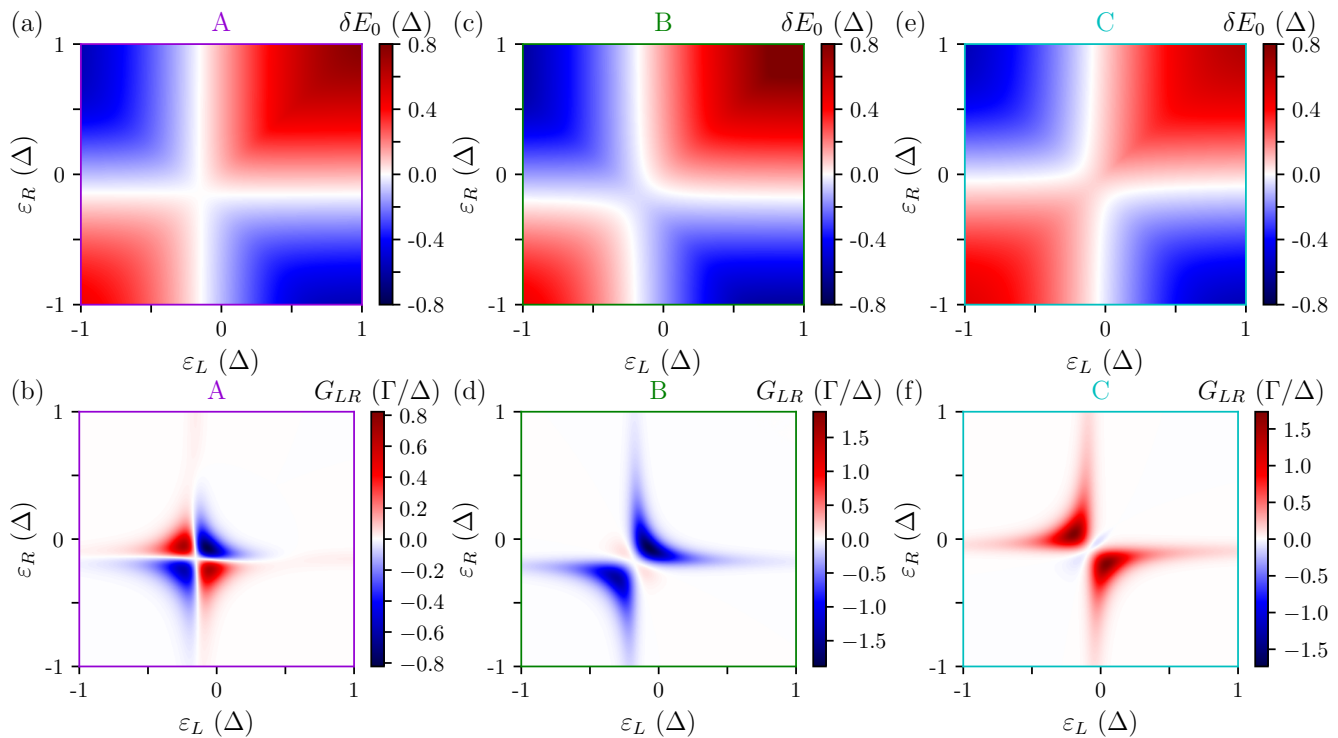


FIG. 3. (a), (c) and (e) Energy difference δE_0 between even and odd parity ground states as a function of ε_L and ε_R , with the same ε_C as in the lines marked A (a), B (c) and C (e) in Fig. 2(a). (b), (d) and (f) Same as (a), (c) and (e), but showing G_{LR} instead.

MBSs in our system, namely their chargeless nature. For that purpose, we calculate

$$\delta Q_{L,R} = \langle O | n_{L,R} | O \rangle - \langle E | n_{L,R} | E \rangle, \quad (5)$$

i.e., the lowest energy even and odd parity states have a charge difference δQ_j on QD j . At the sweet spots in Fig. 2 we find $|\delta Q_{L,R}| \approx 5 \times 10^{-3}$, with significantly larger values away from the sweet spots. In summary, based on our results above, we draw the important conclusion that it is indeed possible to find sweet spots with localized MBSs in our system.

Transport spectroscopy. Next we focus on how to experimentally find the sweet spots with significant MP based on transport spectroscopy. We consider a transport setup according to Fig. 1(a) with QDs L and R coupled with tunnel couplings $\Gamma_L = \Gamma_R = \Gamma$ to normal leads with applied voltages V_L and V_R (the superconductor is kept grounded). The normal leads are kept at temperature $T = \Delta/40$. Focusing on the regime $\Gamma \ll T$, we calculate the current based on first-order rate equations [54, 55]. In this regime, cotunneling, Kondo correlations, and renormalization of the QD energies due to the coupling to the normal leads are negligible.

Figures 3(a), (c) and (e) show δE_0 , just as in Fig. 2(a), but now as a function of ε_L and ε_R with ε_C as in the lines marked A (a), B (c) and C (e) in Fig. 2(a). The local zero-bias conductance, $G_{jj} = dI_j/dV_j$ at $V_L = V_R = 0$, is plotted in the SI [54] and shows peaks along the even-odd degeneracy lines. However, depending on T relative

to the gap to excited states, it can be hard to accurately determine the sweet spot based on a local conductance measurement. It is known that nonlocal conductance, for example $G_{LR} = dI_L/dV_R$, can reveal additional information about subgap states [56–59]. Figures 3(b), (d) and (f) show G_{LR} corresponding to the parameters in Figs. 3(a), (c) and (e). The MBS sweet spot, present only in Fig. 3(b), gives rise to a distinct G_{LR} texture, with $G_{LR} = 0$ at the degeneracy lines which cross at the sweet spot, and equal magnitudes of positive and negative G_{LR} . In contrast, for parameters where there is no sweet spot, zeros of G_{LR} do not coincide with degeneracy lines and G_{LR} is dominated by either positive or negative values. This is in qualitative agreement with the experimental findings in Ref. [44].

Low-quality MBSs. Finally, we investigate how the MBS quality, as quantified by the MP, depends on the different parameters, and how we can avoid being fooled by an apparent sweet spot with low MP (“low-MP sweet spot” in the following). Figure 4(a) shows $|M|$ as a function of $E_Z = E_{ZL} = E_{ZR}$ for different values of U with ε_C and $\varepsilon_L = \varepsilon_R$ adjusted to an even-odd degeneracy with the highest possible $|M|$ (all other parameters are the same as above). For large E_Z we find that $|M| \rightarrow 1$, which is to be expected as the model then approaches the original poor man’s MBS model [35]. Importantly, however, we note that the values of E_Z required for a good MP are much larger than the gap to the nearest excited states which is $\sim 0.15\Delta$ in Fig. 2(c). A large U

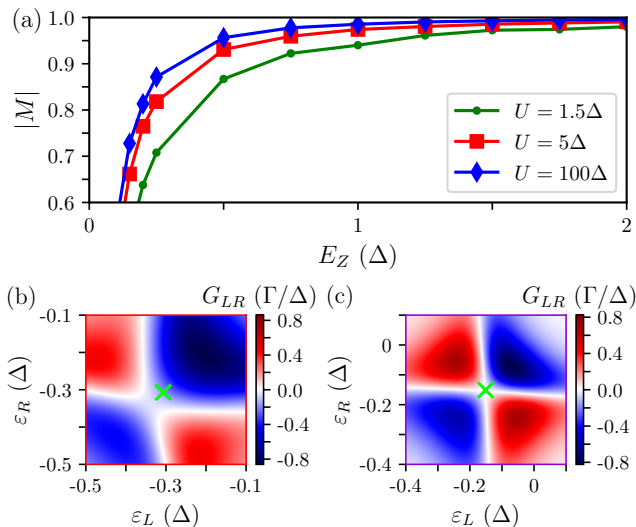


FIG. 4. (a) $|M|$ as a function of E_Z for different U . (b) G_{LR} as a function of ε_L and ε_R for $E_Z = 0.15\Delta$ and $U = 5\Delta$. There is an apparent sweet spot at $\varepsilon_C \approx -0.558\Delta$, $\varepsilon_L = \varepsilon_R \approx -0.316\Delta$ (marked with a green cross) with a low $|M| \approx 0.661$. (c) Same as (b) but for the same parameters as in Fig. 3(a) [zoomed in version of Fig. 3(a)]. At the sweet spot marked with the green cross in (c), $|M| \approx 0.985$.

helps to maintain high MP for smaller E_Z , which is also to be expected as it suppresses local Andreev reflection and prevents double occupation of the outer QDs.

The appearance of low-MP sweet spots presents a challenge for experiments aiming to identify and eventually utilize MBSs. Figure 4(a) shows what to expect for a given set of parameters, but a direct experimental signature that can distinguish between high- and low-MP sweet spots would be desirable. As we show in the SI [54], $\delta E_0(\varepsilon_L, \varepsilon_R, \varepsilon_C)$ (and therefore the local conductances) are rather similar for high- and low-MP sweet spots. We also find a similarly small δQ [see Eq. (5)] for high- and low-MP sweet spots. Fortunately, a distinction can in principle be made based on a measurement of G_{LR} . Fig-

ure 4(b) shows G_{LR} for parameters such that the MP maximum is $|M| \approx 0.661$, while Fig. 4(c) shows the same plot for parameters such that the MP maximum is $|M| \approx 0.985$. For relatively low $|M|$ the zero lines in G_{LR} do not cross, and the avoided crossing does not coincide with the location of the low-MP sweet spot (marked with a green cross). The nonlocal conductance is thus finite at the degeneracy.

Conclusions. In this work, we have considered a system with three QDs for engineering fine-tuned MBSs, the so-called poor man's MBSs. These states require proximity-induced superconductivity on the central QD, spin-orbit coupling between the QDs, Zeeman splitting due to an external field, and fine-tuning of the energies of the QD orbitals. We have quantified the MBS quality using the MP, showing that onsite Coulomb repulsion in the outer dots and Zeeman field increase their quality. A good MBS is characterized by the simultaneous occurrence of a degenerate ground state and a high MP value for the same parameters. In contrast, a bad MBS shows low MP values at the ground state degeneracy. This characteristic leads to different nonlocal transport properties, which can be used to identify high-quality MBSs.

Although the poor man's MBSs are not topologically protected, they preserve the remaining topological properties, including the non-abelian exchange properties. For this reason, they become a promising alternative to experimentally demonstrate the exotic physics of MBSs. Proposals to measure noise [60–63] or entropy [64–67] associated with MBSs, and to measure Majorana fusion [68, 69] and braiding [70–72] are compatible with the present proposal, allowing for a definitive demonstration of the topological superconducting phase.

Acknowledgments. We acknowledge stimulating discussions with M. Nitsch, V. Svensson, O. A. Awoga, S. Matern, A. Danilenko, A. Pöschl, K. Flensberg, and C. M. Marcus, and funding from NanoLund, the Swedish Research Council (VR) and the European Research Council (ERC) under the European Union's Horizon 2020 research and innovation programme under Grant Agreement No. 856526.

-
- [1] J. Alicea, Rep. Prog. Phys. **75**, 076501 (2012).
 - [2] M. Leijnse and K. Flensberg, Semicond. Sci. Technol. **27**, 124003 (2012).
 - [3] R. Aguado, Riv. Nuovo Cimento **40**, 523 (2017).
 - [4] C. W. J. Beenakker, SciPost Phys. Lect. Notes, 15 (2020).
 - [5] C. Nayak, S. H. Simon, A. Stern, M. Freedman, and S. Das Sarma, Rev. Mod. Phys. **80**, 1083 (2008).
 - [6] A. Y. Kitaev, Phys. Usp. **44**, 131 (2001).
 - [7] R. M. Lutchyn, J. D. Sau, and S. Das Sarma, Phys. Rev. Lett. **105**, 077001 (2010).
 - [8] Y. Oreg, G. Refael, and F. von Oppen, Phys. Rev. Lett. **105**, 177002 (2010).
 - [9] S. Nadj-Perge, I. K. Drozdov, B. A. Bernevig, and A. Yazdani, Phys. Rev. B **88**, 020407(R) (2013).
 - [10] M. Hell, M. Leijnse, and K. Flensberg, Phys. Rev. Lett. **118**, 107701 (2017).
 - [11] F. Pientka, A. Keselman, E. Berg, A. Yacoby, A. Stern, and B. I. Halperin, Phys. Rev. X **7**, 021032 (2017).
 - [12] S. Vaitiekėnas, G. W. Winkler, B. van Heck, T. Karzig, M.-T. Deng, K. Flensberg, L. I. Glazman, C. Nayak, P. Krogstrup, R. M. Lutchyn, and C. M. Marcus, Science **367** (2020).
 - [13] K. Flensberg, F. von Oppen, and A. Stern, Nat. Rev. Mater. **6**, 944 (2021).
 - [14] V. Mourik, K. Zuo, S. M. Frolov, S. R. Plissard, E. P. A. M. Bakkers, and L. P. Kouwenhoven, Science **336**, 1003 (2012).
 - [15] M. T. Deng, C. L. Yu, G. Y. Huang, M. Larsson, P. Caroff, and H. Q. Xu, Nano Lett. **12**, 6414 (2012).

- [16] A. D. K. Finck, D. J. Van Harlingen, P. K. Mohseni, K. Jung, and X. Li, *Phys. Rev. Lett.* **110**, 126406 (2013).
- [17] S. Nadj-Perge, I. K. Drozdov, J. Li, H. Chen, S. Jeon, J. Seo, A. H. MacDonald, B. A. Bernevig, and A. Yazdani, *Science* **346**, 602 (2014).
- [18] M. T. Deng, S. Vaitiekėnas, E. B. Hansen, J. Danon, M. Leijnse, K. Flensberg, J. Nygård, P. Krogstrup, and C. M. Marcus, *Science* **354**, 1557 (2016).
- [19] F. Nichele, A. C. C. Drachmann, A. M. Whiticar, E. C. T. O'Farrell, H. J. Suominen, A. Fornieri, T. Wang, G. C. Gardner, C. Thomas, A. T. Hatke, P. Krogstrup, M. J. Manfra, K. Flensberg, and C. M. Marcus, *Phys. Rev. Lett.* **119**, 136803 (2017).
- [20] R. M. Lutchyn, E. P. Bakkers, L. P. Kouwenhoven, P. Krogstrup, C. M. Marcus, and Y. Oreg, *Nat. Rev. Mater.* **3**, 52 (2018).
- [21] A. Fornieri, A. M. Whiticar, F. Setiawan, E. Portolés, A. C. C. Drachmann, A. Keselman, S. Gronin, C. Thomas, T. Wang, R. Kallagher, G. C. Gardner, E. Berg, M. J. Manfra, A. Stern, C. M. Marcus, and F. Nichele, *Nature* **569**, 89 (2019).
- [22] H. Ren, F. Pientka, S. Hart, A. T. Pierce, M. Kosowsky, L. Lunczer, R. Schlereth, B. Scharf, E. M. Hankiewicz, L. W. Molenkamp, B. I. Halperin, and A. Yacoby, *Nature* **569**, 93 (2019).
- [23] E. Prada, P. San-Jose, and R. Aguado, *Phys. Rev. B* **86**, 180503(R) (2012).
- [24] G. Kells, D. Meidan, and P. W. Brouwer, *Phys. Rev. B* **86**, 100503(R) (2012).
- [25] J. Liu, A. C. Potter, K. T. Law, and P. A. Lee, *Phys. Rev. Lett.* **109**, 267002 (2012).
- [26] C.-X. Liu, J. D. Sau, T. D. Stanescu, and S. Das Sarma, *Phys. Rev. B* **96**, 075161 (2017).
- [27] C. Moore, C. Zeng, T. D. Stanescu, and S. Tewari, *Phys. Rev. B* **98**, 155314 (2018).
- [28] C. Reeg, O. Dmytruk, D. Chevallier, D. Loss, and J. Klinovaja, *Phys. Rev. B* **98**, 245407 (2018).
- [29] O. A. Awoga, J. Cayao, and A. M. Black-Schaffer, *Phys. Rev. Lett.* **123**, 117001 (2019).
- [30] A. Vuik, B. Nijholt, A. R. Akhmerov, and M. Wimmer, *SciPost Phys.* **7**, 61 (2019).
- [31] H. Pan and S. Das Sarma, *Phys. Rev. Res.* **2**, 013377 (2020).
- [32] E. Prada, P. San-Jose, M. W. A. de Moor, A. Geresdi, E. J. H. Lee, J. Klinovaja, D. Loss, J. Nygård, R. Aguado, and L. P. Kouwenhoven, *Nature Rev. Phys.* **2**, 575 (2020).
- [33] R. Hess, H. F. Legg, D. Loss, and J. Klinovaja, *Phys. Rev. B* **104**, 075405 (2021).
- [34] J. D. Sau and S. D. Sarma, *Nature Commun.* **3**, 964 (2012).
- [35] M. Leijnse and K. Flensberg, *Phys. Rev. B* **86**, 134528 (2012).
- [36] P. Recher, E. V. Sukhorukov, and D. Loss, *Phys. Rev. B* **63**, 165314 (2001).
- [37] L. Hofstetter, S. Csonka, J. Nygård, and C. Schönberger, *Nature* **461**, 960 (2009).
- [38] L. G. Herrmann, F. Portier, P. Roche, A. L. Yeyati, T. Kontos, and C. Strunk, *Phys. Rev. Lett.* **104**, 026801 (2010).
- [39] G. Fülöp, F. Domínguez, S. d'Hollosy, A. Baumgartner, P. Makk, M. H. Madsen, V. A. Guzenko, J. Nygård, C. Schönberger, A. Levy Yeyati, and S. Csonka, *Phys. Rev. Lett.* **115**, 227003 (2015).
- [40] C.-X. Liu, G. Wang, T. Dvir, and M. Wimmer, arXiv:2203.00107 (2022).
- [41] S. V. Aksenov, A. O. Zlotnikov, and M. S. Shustin, *Phys. Rev. B* **101**, 125431 (2020).
- [42] N. Sedlmayr and C. Bena, *Phys. Rev. B* **92**, 115115 (2015).
- [43] N. Sedlmayr, J. M. Aguiar-Hualde, and C. Bena, *Phys. Rev. B* **93**, 155425 (2016).
- [44] T. Dvir, G. Wang, N. van Loo, C.-X. Liu, G. P. Mazur, A. Bordin, S. L. D. ten Haaf, J.-Y. Wang, D. van Driel, F. Zatelli, X. Li, F. K. Malinowski, S. Gazibegovic, G. Badawy, E. P. A. M. Bakkers, M. Wimmer, and L. P. Kouwenhoven, arXiv:2206.08045 (2022).
- [45] A. Brunetti, A. Zazunov, A. Kundu, and R. Egger, *Phys. Rev. B* **88**, 144515 (2013).
- [46] A. R. Wright and M. Veldhorst, *Phys. Rev. Lett.* **111**, 096801 (2013).
- [47] T. E. O'Brien, A. R. Wright, and M. Veldhorst, *Phys. status solidi* **252**, 1731 (2015).
- [48] D. Stepanenko, M. Rudner, B. I. Halperin, and D. Loss, *Phys. Rev. B* **85**, 075416 (2012).
- [49] M. Governale, M. G. Pala, and J. König, *Phys. Rev. B* **77**, 134513 (2008).
- [50] A. V. Rozhkov and D. P. Arovas, *Phys. Rev. B* **62**, 6687 (2000).
- [51] Y. Tanaka, A. Oguri, and A. C. Hewson, *New J. Phys.* **9**, 115 (2007).
- [52] C. Karrasch, A. Oguri, and V. Meden, *Phys. Rev. B* **77**, 024517 (2008).
- [53] G. Wang, T. Dvir, G. P. Mazur, C.-X. Liu, N. van Loo, S. L. D. ten Haaf, A. Bordin, S. Gazibegovic, G. Badawy, E. P. A. M. Bakkers, M. Wimmer, and L. P. Kouwenhoven, arXiv:2205.03458 (2022).
- [54] See Supplementary Information in (URL included by the Editor) including Refs. [73–77].
- [55] G. Kiršanskas, J. N. Pedersen, O. Karlström, M. Leijnse, and A. Wacker, *Comput. Phys. Commun.* **221**, 317 (2017).
- [56] D. I. Pikulin, B. van Heck, T. Karzig, E. A. Martinez, B. Nijholt, T. Laeven, G. W. Winkler, J. D. Watson, S. Heedt, M. Temurhan, V. Svidenko, R. M. Lutchyn, M. Thomas, G. de Lange, L. Casparis, and C. Nayak, arXiv:2103.12217v1 (2021).
- [57] J. Danon, A. B. Hellenes, E. B. Hansen, L. Casparis, A. P. Higginbotham, and K. Flensberg, *Phys. Rev. Lett.* **124**, 036801 (2020).
- [58] A. Pöschl, A. Danilenko, D. Sabonis, K. Kristjuhan, T. Lindemann, C. Thomas, M. J. Manfra, and C. M. Marcus, arXiv:2204.02430v1 (2022).
- [59] A. Maiani, M. Geier, and K. Flensberg, arXiv:2205.11193v2 (2022).
- [60] D. E. Liu, M. Cheng, and R. M. Lutchyn, *Phys. Rev. B* **91**, 081405(R) (2015).
- [61] D. E. Liu, A. Levchenko, and R. M. Lutchyn, *Phys. Rev. B* **92**, 205422 (2015).
- [62] S. Smirnov, *Phys. Rev. B* **99**, 165427 (2019).
- [63] G.-H. Feng and H.-H. Zhang, *Phys. Rev. B* **105**, 035148 (2022).
- [64] S. Smirnov, *Phys. Rev. B* **92**, 195312 (2015).
- [65] E. Sela, Y. Oreg, S. Plugge, N. Hartman, S. Lüscher, and J. Folk, *Phys. Rev. Lett.* **123**, 147702 (2019).
- [66] S. Smirnov, *Phys. Rev. B* **103**, 075440 (2021).
- [67] C. Han, Z. Iftikhar, Y. Kleeorin, A. Anthore, F. Pierre, Y. Meir, A. K. Mitchell, and E. Sela, *Phys. Rev. Lett.* **128**, 146803 (2022).

- [68] D. Aasen, M. Hell, R. V. Mishmash, A. Higginbotham, J. Danon, M. Leijnse, T. S. Jespersen, J. A. Folk, C. M. Marcus, K. Flensberg, and J. Alicea, *Phys. Rev. X* **6**, 031016 (2016).
- [69] R. S. Souto and M. Leijnse, *SciPost Phys.* **12**, 161 (2022).
- [70] P. Bonderson, M. Freedman, and C. Nayak, *Phys. Rev. Lett.* **101**, 010501 (2008).
- [71] K. Flensberg, *Phys. Rev. Lett.* **106**, 090503 (2011).
- [72] B. van Heck, A. R. Akhmerov, F. Hassler, M. Burrello, and C. W. J. Beenakker, *New J. Phys.* **14**, 035019 (2012).
- [73] K. F. H. Bruus, *Many-Body Quantum Theory in Condensed Matter Physics: An Introduction* (Oxford University Press, 2004).
- [74] K. Grove-Rasmussen, G. Steffensen, A. Jellinggaard, M. H. Madsen, R. Žitko, J. Paaske, and J. Nygård, *Nature Commun.* **9**, 2376 (2018).
- [75] L. Yu, *Acta Phys. Sin.* **21**, 75 (1965).
- [76] H. Shiba, *Prog. Theor. Phys.* **40**, 435 (1968).
- [77] A. I. Rusinov, *JETP Lett.* **9**, 85 (1969).

Supplemental Information to “Creating and detecting poor man’s Majorana bound states in interacting quantum dots”

Athanasios Tsintzis,¹ Rubén Seoane Souto,^{1,2} and Martin Leijnse^{1,2}

¹*Division of Solid State Physics and NanoLund, Lund University, S-221 00 Lund, Sweden*

²*Center for Quantum Devices, Niels Bohr Institute, University of Copenhagen, DK-2100 Copenhagen, Denmark*

Transport theory. Here, we provide the details of the transport theory used in the main text [1], which is based on solving a rate equation for the reduced density matrix of the QD system. The rate equation neglects second and higher order processes in the tunnel coupling Γ between a QD and the leads, which is valid in the regime $\Gamma \ll T$ ($e = \hbar = k_B = 1$). In addition, it assumes the reduced density matrix of the QD system to be diagonal. This is a valid approximation when there are only (quasi-)degeneracies between eigenstates of the QD system that differ by a quantum number that is conserved by the total Hamiltonian, including the leads. In our case, the only such quantum number is the parity of the electron number. Here we motivate the formalism and present a form of the equations that does not rely on charge being a good quantum number in the system.

The full Hamiltonian of the system presented in Fig. 1(a) of the main text is:

$$H = H_{QDs} + \sum_r H_r + H_T, \quad (\text{S1})$$

where H_{QDs} is given in Eq. (1) in the main text and can be written in diagonalized form as $H_{QDs} = \sum_a E_a |a\rangle \langle a|$, with many-body eigenenergies E_a and eigenstates $|a\rangle$ of definite parity. Note that charge is not a good quantum number because H_{QDs} includes superconducting proximity effect on QD C . $\sum_r H_r$ is the sum of the normal (N) leads Hamiltonians ($r = L, R$) and H_T contains the couplings between the N leads and the QDs. H_r and H_T are given by:

$$H_r = \sum_{k\sigma} \varepsilon_{rk\sigma} c_{rk\sigma}^\dagger c_{rk\sigma}, \quad (\text{S2})$$

$$H_T = \sum_{rk\sigma a} \left[T_{r\sigma+}^{aa'} |a\rangle \langle a'| c_{rk\sigma} - T_{r\sigma-}^{aa'} |a\rangle \langle a'| c_{rk\sigma}^\dagger \right]. \quad (\text{S3})$$

The operator $c_{rk\sigma}^\dagger$ creates an electron with spin σ in momentum state k in lead r and $\varepsilon_{rk\sigma}$ is the corresponding electron energy. The transition matrix elements from QD state $|a'\rangle$ to $|a\rangle$, $T_{r\sigma+(-)}^{aa'}$, are given by the expressions:

$$T_{r\sigma+}^{aa'} = \sum_{j \neq C} \lambda_{rj\sigma} \langle a | d_{j\sigma}^\dagger | a' \rangle, \quad (\text{S4})$$

$$T_{r\sigma-}^{aa'} = \sum_{j \neq C} \lambda_{rj\sigma}^* \langle a | d_{j\sigma} | a' \rangle = (T_{r\sigma+}^{a'a})^*, \quad (\text{S5})$$

where $\lambda_{rj\sigma}$ parametrizes the tunnel coupling between QD $j = L, R$ and lead r . The tunnel couplings can be calcu-

lated using Fermi’s golden rule [2]:

$$\Gamma_{r\sigma+(-)}^{aa'} = 2\pi \rho_r |T_{r\sigma+(-)}^{aa'}|^2, \quad (\text{S6})$$

where the density of states ρ_r is taken to be energy-independent. The tunneling rates for jumping into and out of the QD are given by

$$W_{\sigma+}^{aa'} = \sum_r \Gamma_{r\sigma+}^{aa'} f_r(E_a - E_{a'}) = \sum_r W_{r\sigma+}^{aa'}, \quad (\text{S7})$$

$$W_{\sigma-}^{aa'} = \sum_r \Gamma_{r\sigma-}^{aa'} [1 - f_r(E_{a'} - E_a)] = \sum_r W_{r\sigma-}^{aa'}, \quad (\text{S8})$$

where $f_r(x)$ is the Fermi function. The diagonal elements of the QD system’s reduced density matrix are the occupation probabilities P_a of the eigenstates $|a\rangle$, and their time dependence is given by:

$$\dot{P}_a = \sum_{\sigma a'} [W_{\sigma+}^{aa'} + W_{\sigma-}^{aa'}] P_{a'} - \sum_{\sigma a'} [W_{\sigma+}^{a'a} + W_{\sigma-}^{a'a}] P_a. \quad (\text{S9})$$

Note that the system can transition from state $|a'\rangle$ to state $|a\rangle$ both by adding (+) and removing (−) an electron to/from the QDs because charge is not a good quantum number. The set of Eqs. (S9) is solved for the steady state, $\dot{P}_a = 0$, together with the normalization condition $\sum_a P_a = 1$. The particle current flowing out of lead r can be expressed by counting particles tunnelling into the QD system minus particles tunnelling out of the QD system, weighted by the probabilities of the initial states:

$$I_r = \sum_{\sigma a a'} (W_{r\sigma+}^{aa'} - W_{r\sigma-}^{aa'}) P_{a'}. \quad (\text{S10})$$

Additional conductance plots. In the transport setup in Fig. 1 in the main text, we apply voltages V_r to the two normal leads $r = L, R$. Because of the grounded superconducting lead (entering H_{QDs} through pairing terms on QD C), $I_L \neq -I_R$ in general, and we calculate the currents $I_r(V_L, V_R)$ and conductances

$$G_{rr'}(V_L, V_R) = \frac{dI_r(V_L, V_R)}{dV_{r'}}. \quad (\text{S11})$$

In the main text, Figs. 3(b, d, f) and Figs. 4(b, c) show the linear nonlocal conductance

$$G_{LR} = G_{LR}(0, 0), \quad (\text{S12})$$

where we have introduced the notation $G_{rr'}(0, 0) = G_{rr'}$.

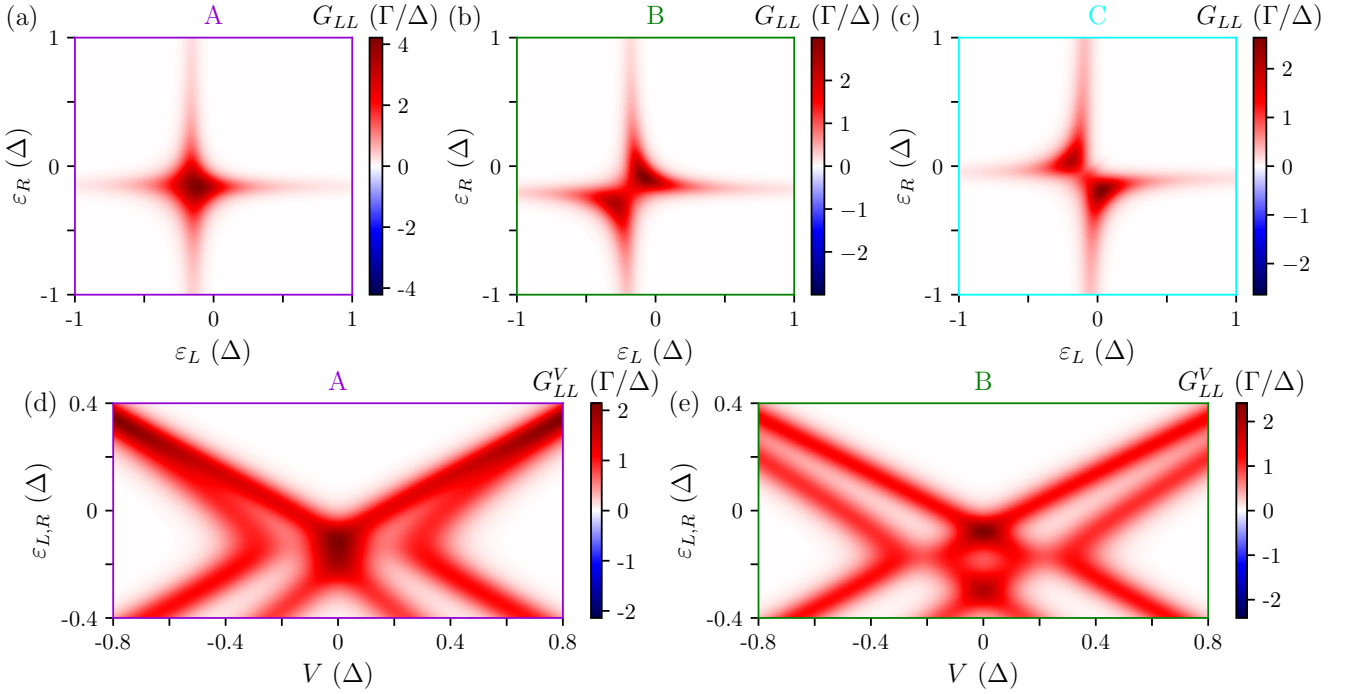


FIG. S1. (a), (b) and (c) Local linear conductance G_{LL} as a function of ε_L and ε_R , with the same ε_C as in Figs. 3(a, c, e) of the main text. (d) and (e) Local nonlinear conductance G_{LL}^V as a function of $\varepsilon_L = \varepsilon_R$ and bias voltage V with the same ε_C as in (a) [(d)] and (b) [(e)].

Here, we show in Figs. S1(a, b, c) G_{LL} as a function of ε_L and ε_R for ε_C values fixed by the cuts A, B and C in Figs. 3(a, c, e) of the main text. G_{LL} shows peaks along the even-odd degeneracy lines. The nonlinear local conductance $G_{LL}^V = G_{LL}(V/2, -V/2)$ as a function of $\varepsilon_L = \varepsilon_R$ and a bias voltage V for ε_C corresponding to (a) and (b) is depicted in (d) and (e). The finite V conductance lines reflect the excitation energies shown in Figs. 2(c) and (d) of the main text.

Sweet spots for different spin-orbit coupling strengths. A significant spin-orbit interaction is a necessary ingredient to realize MBSs in the proposed system, as it provides a spin-flipping mechanism for electrons hopping between the QDs. Without spin-orbit coupling, H_{QDs} would be diagonal in spin and there would be no CAR involving the lowest spin states on QDs L and R . It is thus important to investigate the effect of a varying strength of the spin-orbit coupling on the quality of the MBSs, both in terms of the MP and the gap to the excited states. Similarly to Fig. 2(a) in the main text, Figs. S2(a, b) show $\delta E_0 = E^O - E^E$, the energy difference between the odd and even parity ground states, as a function of ε_C and $\varepsilon_L = \varepsilon_R$, but for a larger and smaller spin-orbit coupling strength [$t_{SO} = 0.3t$ in (a) and $t_{SO} = 0.1t$ in (b)]. The cuts (lines) passing through the sweet spots (crosses) are marked with purple and green in (a) and (b) respectively. Like in Fig. 2(c) in the main text, Figs. S2(c) and (d) show $|M|$ together with $|\delta E_0|$ and the excitation energies above the global ground state ($|\delta E_n|, n \geq 1$) as a function of $\varepsilon_L = \varepsilon_R$ corresponding to the values

of ε_C marked with the lines in (a) and (b) [purple and green]. The peaks of $|M|$ occur at the same $\varepsilon_{L,R}$ as the ground state degeneracies in both (c) and (d), which implies high-MP sweet spots [$|M| > 0.985$ in both (c) and (d)]. There exists a striking difference in the excitation energies though. While in (c) the lowest excitation is at around 0.2Δ - which is higher than the one presented in the main text - in (d) the excitation gap is smaller than 0.1Δ . The reason for this dependence is that the couplings within the even parity sector are limited by the spin-orbit coupling strength. At the sweet spot, ε_C has been adjusted to make the couplings in the even and odd sectors similar. These couplings set the distance to the lowest excited states. A good separation to the excited states (typically $\delta E_1 \gg T$) is required for MBS detection, as well as for qubit-like operations and nonabelian and nonlocal protocols.

Low-MP sweet spots. In this part we provide additional information on the low-MP sweet spot whose non-local conductance is explored in Fig. 4(b) of the main text. Figure S3(a) is similar to Fig. 2(a) of the main text but with $E_Z = 0.15\Delta$. The low-MP sweet spot is marked with a purple cross and the excitation energies together with $|M|$ along the cut (purple line) are plotted in Fig. S3(b). From the latter figure, it is clear that the peak of $|M|$ is not as pronounced as in Fig. 2(c) of the main text. More importantly, the even-odd degeneracy point does not coincide with the $|M|$ peak and corresponds to an even smaller $|M| \approx 0.661$. Additionally, the excitation gap is smaller than 0.1Δ . The above features

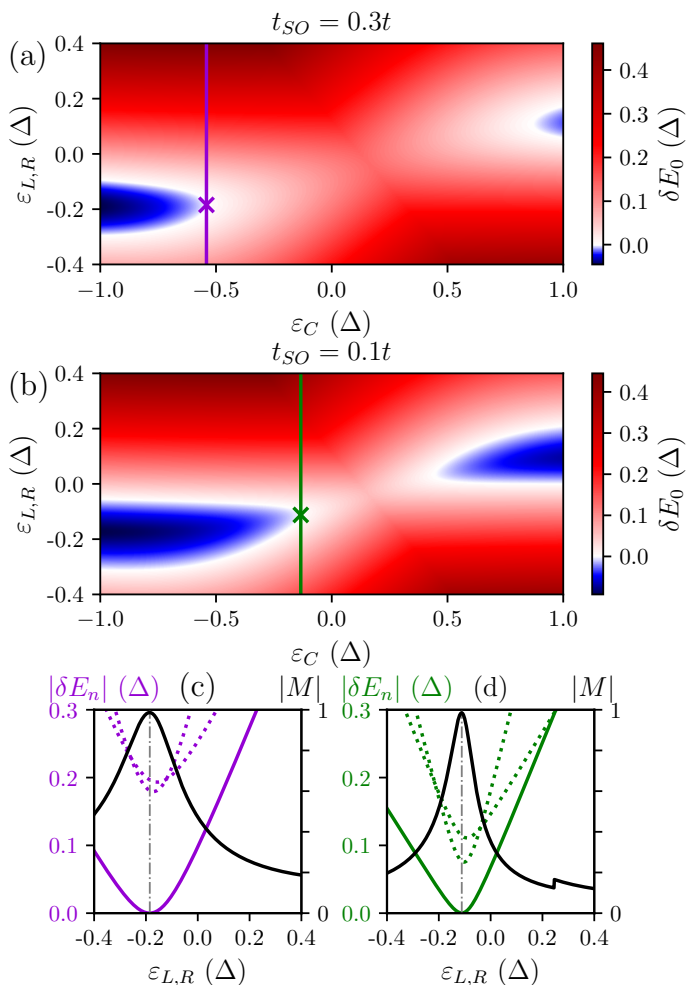


FIG. S2. (a) and (b) δE_0 as a function of $\varepsilon_L = \varepsilon_R$ and ε_C for $t_{SO} = 0.3t$ and $t_{SO} = 0.1t$ respectively. The cuts [purple line for (a) and green line for (b)] are explored in (c) and (d). The purple cross in (a) marks the sweet spot at $\varepsilon_C \approx -0.541\Delta$, $\varepsilon_L = \varepsilon_R \approx -0.185\Delta$, while the sweet spot in (b) is marked by the green cross at $\varepsilon_C \approx -0.134\Delta$, $\varepsilon_L = \varepsilon_R \approx -0.112\Delta$. (c) $|\delta E_n|$ (left axis, purple lines) as a function of $\varepsilon_L = \varepsilon_R$ along the cut in (a) (purple line). The lowest excited state (full line) has different parity (odd in this case) than the ground state (even in this case); one of the two higher excited states shown (dotted lines) has even parity and the other odd. The black line shows $|M|$ (right axis) as a function of $\varepsilon_L = \varepsilon_R$ along the cut in (a). (d) Same as (c) but along the cut in (b) (green line). The vertical dash-dotted lines in (c) and (d) indicate the maximum of $|M|$.

are characteristic for low-quality MBSs. In Fig. S3(c) we plot the difference between the energies of the even and odd ground states ($\delta E_0 = E^0 - E^E$) as a function of ε_L and ε_R . The degeneracy lines do cross but are not straight as in Fig. 3(a) in the main text. This means that the ground state degeneracy is not entirely protected from small changes of $\varepsilon_{L,R}$. We note that these features would probably be hard to discern with local conductance measurements.

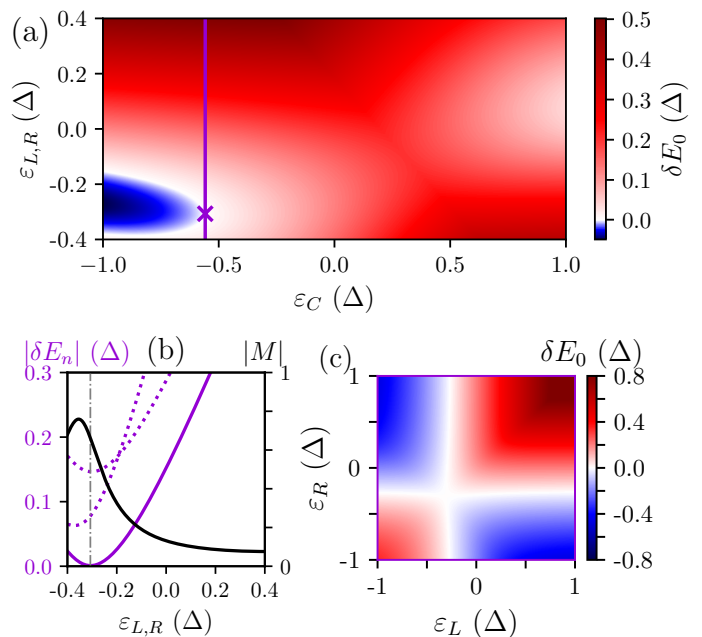


FIG. S3. (a) δE_0 as a function of $\varepsilon_L = \varepsilon_R$ and ε_C for $E_Z = 0.15\Delta$ and $U = 5\Delta$. The cut (purple line) is explored in (b). The purple cross marks the low-MP sweet spot at $\varepsilon_C \approx -0.558\Delta$, $\varepsilon_L = \varepsilon_R \approx -0.316\Delta$. (b) $|\delta E_n|$ (left axis, purple lines) as a function of $\varepsilon_L = \varepsilon_R$ along the cut in (a) (purple line). The lowest excited state (full line) has different parity (odd in this case) than the ground state (even in this case); one of the two higher excited states shown (dotted lines) has even parity and the other odd. The black line shows $|M|$ (right axis) as a function of $\varepsilon_L = \varepsilon_R$ along the cut in (a). The vertical dash-dotted line in (b) indicates the misalignment between the points of maximum $|M|$ and of ground state degeneracy. (c) Energy difference δE_0 between even and odd parity ground states as a function of ε_L and ε_R , with the same ε_C as in the purple line in (a).

Sweet spots for finite U_C , E_{ZC} . For the results presented in the main text, we have considered a complete quenching of the Coulomb interactions and Zeeman splitting in QD C ($U_C, E_{ZC} = 0$), due to the strong coupling to the superconductor. Here, we separately study the effects of finite U_C, E_{ZC} on the MBSs quality.

Figures S4(a) and (b) show δE_0 as a function of ε_C and $\varepsilon_L = \varepsilon_R$ for $U_C = 0.5\Delta$ and $U_C = \Delta$, respectively ($E_{ZC} = 0$). The cuts (lines) passing through the sweet spots (crosses) are marked with purple in (a) and green in (b). Figures S4(c) and (d) show $|M|$ together with $|\delta E_0|$ and the excitation energies above the global ground state ($|\delta E_n|, n \geq 1$) as a function of $\varepsilon_L = \varepsilon_R$ corresponding to the values of ε_C marked with the lines in (a) and (b) (purple and green). The peaks of $|M|$ occur at the same $\varepsilon_{L,R}$ as the ground state degeneracies in both (c) and (d), which implies high-MP sweet spots ($|M| \approx 0.98$ and $|M| \approx 0.967$). The $|M|$ peaks are not as pronounced as in Fig. 2(c) of the main text ($|M| \approx 0.986$), but the gap to the excited states is in fact enhanced [$|\delta E_1| \approx 0.2\Delta$ in (d)]. Finite (but small) Coulomb interactions in QD

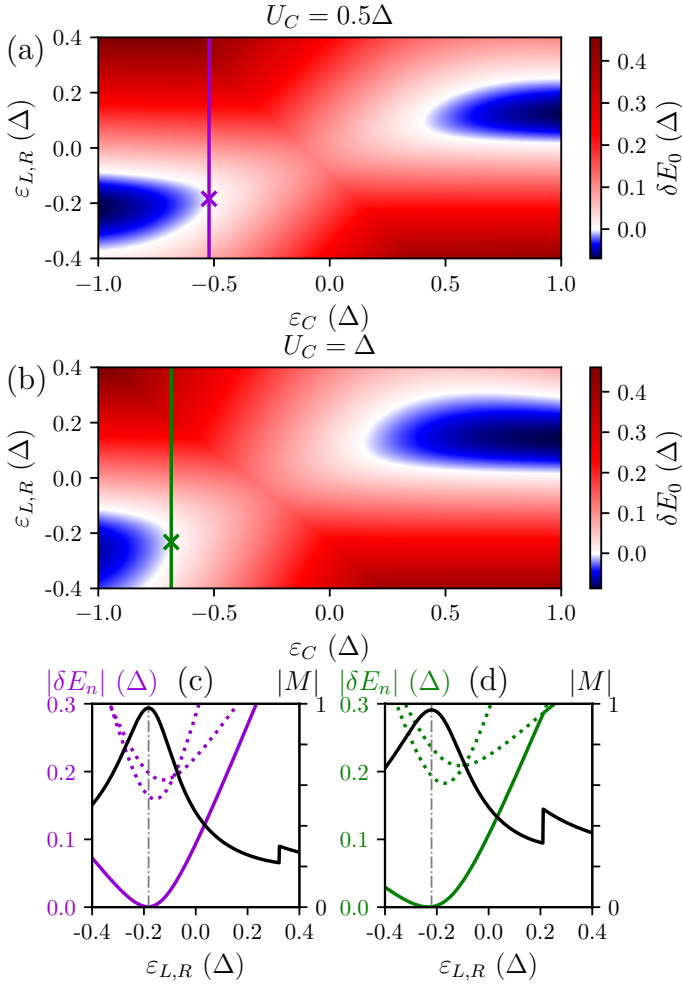


FIG. S4. (a) and (b) δE_0 as a function of $\varepsilon_L = \varepsilon_R$ and ε_C for $U_C = 0.5\Delta$ in (a) and $U_C = \Delta$ in (b) ($E_{ZC} = 0$). The cuts [purple line for (a) and green line for (b)] are explored in (c) and (d). The purple cross in (a) marks the sweet spot at $\varepsilon_C \approx -0.522\Delta$, $\varepsilon_L = \varepsilon_R \approx -0.184\Delta$, while the sweet spot in (b) is marked by the green cross at $\varepsilon_C \approx -0.685\Delta$, $\varepsilon_L = \varepsilon_R \approx -0.232\Delta$. (c) $|\delta E_n|$ (left axis, purple lines) as a function of $\varepsilon_L = \varepsilon_R$ along the cut in (a) (purple line). The lowest excited state (full line) has different parity (odd in this case) than the ground state (even in this case); one of the two higher excited states shown (dotted lines) has even parity and the other odd. The black line shows $|M|$ (right axis) as a function of $\varepsilon_L = \varepsilon_R$ along the cut in (a). (d) Same as (c) but along the cut in (b) (green line). The vertical dash-dotted lines in (c) and (d) indicate the maximum of $|M|$.

C can thus even be advantageous, as they provide a better separation between the ground state and the excited states without significantly disturbing the MBSs localization, as quantified by the MP. We have also verified that the results remain qualitatively unchanged in the presence of interdot Coulomb interactions.

Figures S5(a) and (b) show δE_0 as a function of ε_C and $\varepsilon_L = \varepsilon_R$ for $E_{ZC} = 0.5\Delta$ and $E_{ZC} = \Delta$, respectively ($U_C = 0$). The cuts (lines) passing through the sweet

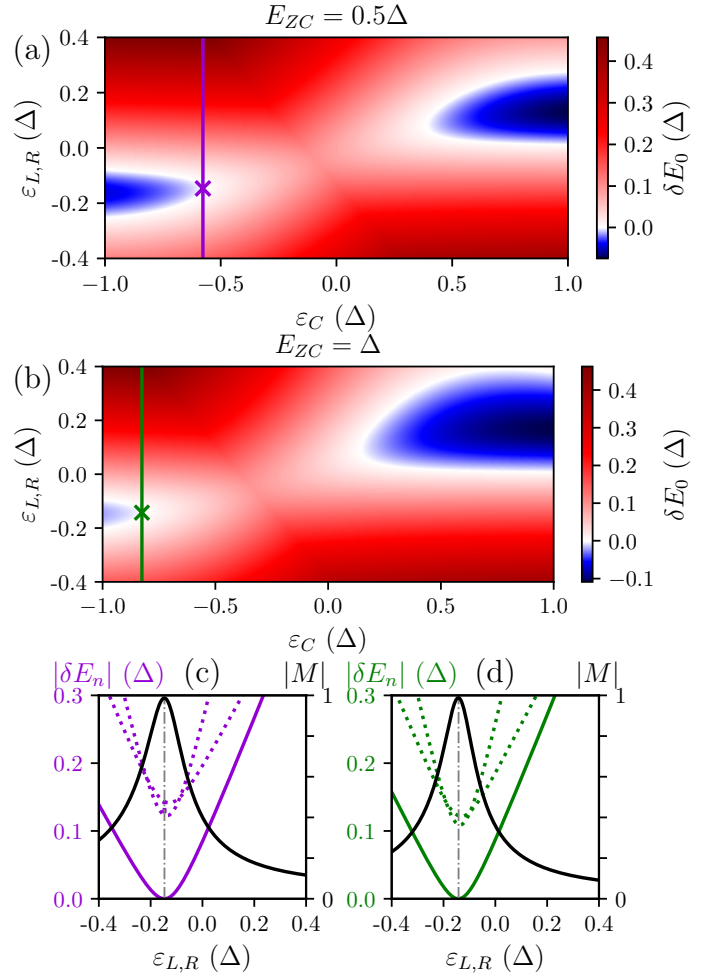


FIG. S5. (a) and (b) δE_0 as a function of $\varepsilon_L = \varepsilon_R$ and ε_C for $E_{ZC} = 0.5\Delta$ in (a) and $E_{ZC} = \Delta$ in (b) ($U_C = 0$). The cuts [purple line for (a) and green line for (b)] are explored in (c) and (d). The purple cross in (a) marks the sweet spot at $\varepsilon_C \approx -0.577\Delta$, $\varepsilon_L = \varepsilon_R \approx -0.147\Delta$, while the sweet spot in (b) is marked by the green cross at $\varepsilon_C \approx -0.826\Delta$, $\varepsilon_L = \varepsilon_R \approx -0.143\Delta$. (c) $|\delta E_n|$ (left axis, purple lines) as a function of $\varepsilon_L = \varepsilon_R$ along the cut in (a) (purple line). The lowest excited state (full line) has different parity (odd in this case) than the ground state (even in this case); one of the two higher excited states shown (dotted lines) has even parity and the other odd. The black line shows $|M|$ (right axis) as a function of $\varepsilon_L = \varepsilon_R$ along the cut in (a). (d) Same as (c) but along the cut in (b) (green line). The vertical dash-dotted lines in (c) and (d) indicate the maximum of $|M|$.

spots (crosses) are marked with purple in (a) and green in (b). Figures S5(c) and (d) show $|M|$ together with $|\delta E_0|$ and the excitation energies above the global ground state ($|\delta E_n|$, $n \geq 1$) as a function of $\varepsilon_L = \varepsilon_R$ corresponding to the values of ε_C marked with the lines in (a) and (b) (purple and green). The peaks of $|M|$ occur at the same $\varepsilon_{L,R}$ as the ground state degeneracies in both (c) and (d), which implies high-MP sweet spots ($|M| \approx 0.987$ and $|M| \approx 0.988$). The $|M|$ peaks are as pronounced as in Fig. 2(c) of the main text, but the gap to the excited

states is slightly reduced.

Emergence of Yu-Shiba-Rusinov states. We note that Yu-Shiba-Rusinov (YSR) states [3–5] can be induced by the couplings of QDs L and R to the proximitized QD C . This physics is included in our calculations because we diagonalize the Hamiltonian of the three coupled QDs exactly. However, because of the strong coupling between the QDs, all states are strongly mixed and we do not find it useful to attempt to identify certain states as YSR-like. It is important to emphasize, however, that YSR physics related to the couplings of QDs L and R to QD C does not prevent the appearance of MBSs.

Possible YSR physics related to the coupling of QD C to the bulk superconductor is, on the other hand, not included in the model because we consider the infinite gap limit for the bulk superconductor. The results presented in the main text are obtained for $E_{ZC} = U_C = 0$, in which case the coupling between QD C and the bulk superconductor does not lead to YSR states. They might, however, become important for large enough E_{ZC} and U_C . Our statements above and in the main text that our

results remain qualitatively unchanged by finite E_{ZC} , U_C are only verified for parameters small enough to not induce YSR states on QD C . Our expectation is, however, that such YSR states would not prevent the appearance of MBSs, as long as they do not approach zero energy, but they might change the exact value of ε_C where the sweet spot appears. What is required for MBSs is just that the states in QD C that mediate the couplings between QDs L and R do so in a way that is different in the even and odd parity subspaces, and that this difference can be controlled (for example by a gate voltage).

Sweet spots for an asymmetric system. In the main text we have considered a symmetric system, $t_L = t_R = t$, $t_L^{SO} = t_R^{SO} = t_{SO}$, $U_L = U_R = U$ and we have only presented MP results for $\varepsilon_L = \varepsilon_R$. Introducing any asymmetry, the definition of MP remains valid but $|M_L| \neq |M_R|$. A different value of the MP in the two QDs should be interpreted as a different degree of localization of the two MBSs. The sweet spots are then found at points where $\varepsilon_L \neq \varepsilon_R$. $|M_L|$ and $|M_R|$ can still come very close to 1 at those sweet spots, but they are not completely identical.

-
- [1] G. Kiršanskas, J. N. Pedersen, O. Karlström, M. Leijnse, and A. Wacker, *Comput. Phys. Commun.* **221**, 317 (2017).
 [2] K. F. H. Bruus, *Many-Body Quantum Theory in Condensed Matter Physics: An Introduction* (Oxford Univer-

- sity Press, 2004).
 [3] L. Yu, *Acta Phys. Sin.* **21**, 75 (1965).
 [4] H. Shiba, *Prog. Theor. Phys.* **40**, 435 (1968).
 [5] A. I. Rusinov, *JETP Lett.* **9**, 85 (1969).